RILEM-*fib*-AFGC Int. Symposium on Ultra-High Performance Fiber-Reinforced Concrete,
UHPFRC 2013 – October 1-3, 2013, Marseille, France

DOWEL ACTION AND SHEAR STRENGTH CONTRIBUTION OF HIGH STRENGTH REBAR EMBEDDED IN ULTRA-HIGH PERFORMANCE FIBER REINFORCED CONCRETE

Yulin Xiao (1), Jun Xia (1), Kevin Mackie (1) and Amir Mirmiran (2)

(1) Civ., Env. & Constr. Engineering Department, University of Central Florida, USA
(2) College of Engineering and Computing, Florida International University, USA

Abstract

Dowel action influence is usually ignored during normal reinforced concrete beam designs since vertical shear reinforcing bars always offer significant shear resistance. However, for Ultra-high Performance Concrete (UHPC) beams without shear reinforcement, the dowel action contribution to the shear strength becomes considerable. Its contribution is also important in assuring a non-brittle type of shear failure. The embedded longitudinal rebar can bridge the bottom cracks and transfer the shear force by bearing on concrete core one side and supported by the UHPC in tension on the other side. A series of notched reinforced dowel specimens were tested to verify the contribution from dowel action with interfacial bond between UHPC and rebar eliminated by using plastic tubes around embedded rebar in UHPC. Important dowel action contributions parameters were obtained and the load versus displacement curve was used to calibrate beam on elastic foundation and finite element models.

Résumé

L'effet de goujon est généralement négligé dans le dimensionnement de poutres en béton armé ordinaire, car les étriers verticaux présentent toujours une résistance au cisaillement significative. Mais, pour des poutres en béton fibré ultra-performant (BFUP), sans armature de cisaillement, la contribution de l'effet de goujon devient considérable. Cette contribution est également importante pour éviter une rupture fragile au cisaillement. L'armature longitudinale intégrée peut ponter les fissures inférieures et transmettre les efforts de cisaillement en s'appuyant sur le noyau de béton d'une part, et sur la résistance à la traction du BFUP, d'autre part. Une série d'essais fut effectuée sur des échantillons entaillés, afin de déterminer la contribution de l'effet de goujon, en éliminant l'adhérence entre le BFUP et les armatures longitudinales par des tubes en plastique. Les paramètres importants de l'effet de goujon ont été mis en évidence. La courbe force-déformation fut utilisée pour calibrer une poutre sur fondation élastique et des modèles d'éléments finis.

1. INTRODUCTION

Due to maintenance, operational, and safety concerns with open grid steel deck system that are commonly used in moveable bridges in Florida, USA, several alternative deck systems were previously investigated [1, 2]. One of them utilized ultra-high performance concrete (UHPC) in passively-reinforced beams without shear reinforcement to lower self-weight of the deck. The typical properties of UHPC are known through mechanical experiments done by researchers previously [3]. The compressive strength of UHPC can reach around 221 *MPa* if manufacturer-recommended heat treatment process is applied and tensile strength can reach up to 10.8 *MPa* [4].

The shear force in beams is mainly transferred by two mechanisms for normal strength concrete (NSC). One is the shear contribution from concrete portion in compression zone and the other is from the effects of aggregate interlocking. Due to the existence of the shear reinforcement, the NSC beam under 3-points bending test usually exhibits flexural failure with widened crack at the middle span. However, for beams made of UHPC, the situation is different. Due to the absence of the coarse aggregates and existence of the fibers, the shear can be transferred by three main mechanisms as shown in Figure 1. The failure model for the conventional 3-points bending test was basically the shear failure when there is no shear reinforcement. Because UHPC has considerable tensile strength, very high post-crack strength, and good bond strength with the longitudinal reinforcement, the flexural cracks width can be fully controlled while the shear cracks are free to develop due to the lack of reinforcement crossing the cracking plane. Hence, the dowel action contribution is worthy an investigation, because the dowel force can be fully activated due to the localized deformation at shear cracks. Generally, the total shear resistance can be expressed as follows in Eq.(1), in which dowel action contribution towards the total loading capacity is considered explicitly. The estimation of peak dowel force and its critical influential factors are worth investigation to obtain a better estimation of the shear strength of the un-shear-reinforced UHPC beams.

$$V = Vc + Vd + Va \tag{1}$$

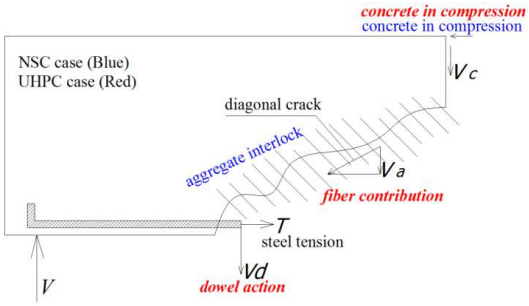

Figure 1: Mechanism of shear transfer

Previous research on dowel action with regard to NSC revealed that the shear capacity of dowel specimen is particularly influenced by the four design parameters: compressive strength of concrete, yielding strength of steel, inclination angle of transverse reinforcement and size of dowel rebar [5, 6]. The contribution of the dowel action to the total shear capacity of a cracked reinforced concrete specimen increases with the value of ρf_y [7], in which ρ is the reinforcement ratio and f_y is the yielding stress of the reinforcement. It also increases

with decreases of rebar diameter. Several test setups aimed at dowel action were summarized by Soroushian [8]. Among them, the double L-shape specimen was usually used to investigate the dowel action against the concrete cover, while the bearing test was usually used to get the response of the rebar again the concrete core. However, the real working condition of longitudinal rebar embedded in the bending beam with diagonal shear cracks is not represented in these tests. Analytically, a simplified model from Friberg [9] is widely used to predict the elastic response of the dowel action. The model treated the rebar as a semi-infinite beam on elastic foundation under a concentrated load. The foundation properties were calculated based on concrete properties. Several curve fitting equations were reported to estimate the ultimate dowel load and displacement and some of these formulas were summarized by Reineck [10] and He [11]. However, most of the equations were fitted using test results from NSC, and the application of these existing equations likely requires adjustments due to the particularity of UHPC.

The objective of this paper is to investigate the dowel action behavior between UHPC and longitudinal high strength reinforcement by means of mechanical tests, theoretical analysis, and finite element simulation.

2. EXPERIMENT

Five groups of notched UHPC prisms reinforced with high strength MMFX rebar were constructed as shown in the following Figure 2 with dimensions for group 1 specimens shown in Figure 3. The notch is 50.8 *mm* wide at rebar locations for all specimens.

Figure 2: Specimen design details

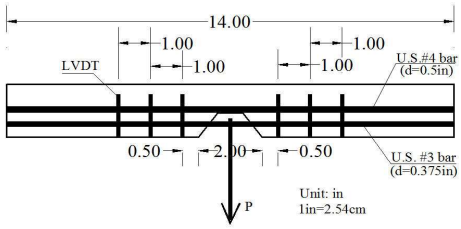

Figure 3: Dimension for Specimen Group 1

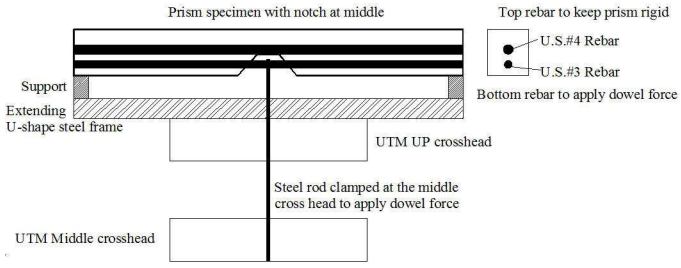

Figure 4: Detailed specimen test setup

Variations of the specimens among different groups, such as length, depth, side and bottom cover, and rebar size are listed in Table 1. In order to prevent the interface bond between UHPC and MMFX rebar, plastic tubes were used to debond the rebar portion embedded in UHPC on both sides of the notches. One No. 4 MMFX rebar was placed above the notch to ensure the rigidity of the top portion of the specimens and prevent the cracks developing

above the notches. The loading was applied by a steel hook clamped at the center of the rebar with the other end of the hook clamped by the UTM. Tensile force was applied pointing downwards as show in Figure 4 using displacement control. Six extensometers were attached to the specimen surface on both sides of the notch. Concrete cubes were cast for each batch and tested. A total of 14 specimens with average age 55 days were tested, and the compressive strength summarized in Table 2.

Table 1: Designed specimen with comparison groups

Specimen group ID	Prism length L (*cm*)	Prism height H (*cm*)	Prism width B (*cm*)	Bond length Lb (*cm*)	Bottom cover (*cm*)	Side cover (*cm*)	Steel bar size db (*cm*)
1	35.6	10.8	3.8	30.5	2.5	1.4	#3 (1.0)
2	**45.7**	10.8	3.8	40.6	2.5	1.4	#3 (1.0)
3	35.6	10.2	3.8	30.5	**1.9**	1.4	#3 (1.0)
4	35.6	10.8	2.9	30.5	2.5	**1.0**	#3 (1.0)
5	35.6	11.4	4.4	30.5	2.5	1.4	**#4 (1.3)**

Table 2: Batches tested for obtaining general compression strength of specimen

Pour	Batch info			
	Batch age upon testing	Size (*cm*) ($a \times b \times c$)	f_c' (*MPa*)	Average/Max f_c' (*MPa*)
1st	60 days	4.45×3.18×3.81	150	133/168*
	60 days	4.45×3.18×4.06	168	
	60 days	4.32×3.56×3.81	135	
	60 days	4.45×3.81×4.06	135	
	60 days	4.45×3.81×4.06	112	
	60 days	4.13×3.81×4.45	101	
2nd	51 days	4.57×3.81×7.62	116	123/139
	51 days	3.81×3.18×4.45	103	
	51 days	3.81×3.18×4.45	139	
	51 days	3.18×2.54×3.18	116	
	51 days	3.68×2.86×4.06	124	
	51 days	3.81×3.30×3.18	139	
	51 days	3.18×2.54×3.51	119	
	51 days	4.83×3.68×4.95	133	

* Maximum number of f_c' was used as the compression strength for any further calculation due to the fact that the cubes were tested without surface grinding.

The progression of failure in a typical specimen is demonstrated in Figure 5. The dowel load increased rapidly initially until the first few cracks appeared at both sides of the notch. After that, the dowel load increased slowly with lower stiffness and the cracks widened on both sides. The specimen reached its peak load shortly after the visibility of the side cracks.

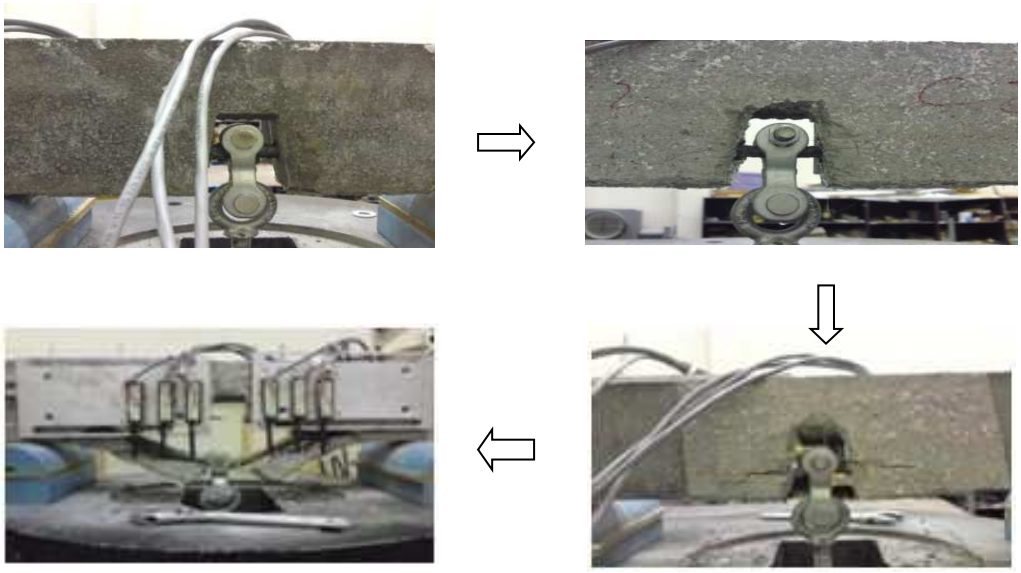

Figure 5: Failure mode of typical specimen

3. THEORETICAL ANALYSIS

3.1 Beam on elastic foundation (BEF)

The experiment setup and corresponding simplified model are shown in Figure 6. The embedded rebar was treated as an elastic beam, while the support from surrounding UHPC was treated as two separate finite length elastic foundations. Because the model is symmetric, only the right part of the beam was considered in the analytical model. The width of the free span L_d in the middle equals the width of the dent $2d$. The approximate solution of this system is listed in the two domains in Eq. (2) based on the approximate equation of the portion 3 from the book. [12]

$$\begin{cases} y_1 = \dfrac{1}{6}c_1x^3 + \dfrac{1}{2}c_2x^2 + c_3x + c_4 & x \in (0, d] \\ y_3 = \dfrac{P_0\beta}{4k}\begin{bmatrix} 4e^{[-\beta(x-d)]}\cos\left[\beta\left(x-d\right)\right] \\ -(2-\beta L_d)e^{[-\beta(x-d)]}\left(\cos(\left[\beta\left(x-d\right)\right]) - \sin(\left[\beta\left(x-d\right)\right])\right) \end{bmatrix} & x \in \left(d, d+L_0\right) \end{cases} \tag{2}$$

where $\beta = \sqrt[4]{\dfrac{k}{4EI}}$

The boundary conditions can be expressed as follows:

$$y_1\left(x=d\right) = y_3\left(x=d\right), \frac{dy_1}{dx}\left(x=d\right) = \frac{dy_3}{dx}\left(x=d\right), \frac{dy_1}{dx}\left(x=0\right) = 0, -EI\frac{d^3y_1}{dx^3}\left(x=0\right) + \frac{P}{2} = 0 \tag{3}$$

By solving these equations, the final displacement expressions are

$$\begin{cases} y_1 = \dfrac{P_0}{24EIkd}(2x^3kd - 6x^2EI\beta^3L_d - 3x^2d^2k + 6d^2EI\beta^3L_d + 12dEI\beta + 6dEI\beta^2L_d + d^4k) \\ y_3 = \dfrac{P_0}{4k}\beta e^{(\beta(-x+d))}\left[2\cos(\beta(-x+d)) - 2\sin(\beta(-x+d)) + \beta L_d\cos(\beta(-x+d)) + \beta L_d\sin(\beta(-x+d))\right] \end{cases} \tag{4}$$

The elastic solution is valid only before the initiation of the cracks. After that, the UHPC cover will lose stiffness at the crack location and the foundation modulus will no longer be uniform along the length of beam. Because at such an early loading stage, the extensometers at locations L3.5 and L2.5 did not show any significant deformations, only recorded data at location L1.5 are used for the calibrations. The expressions of foundation deformation were coded in Matlab and nonlinear curve fitting were performed using a load range of 5%-40% of the peak load. The curve fitting results are summarized in the following Table 3. Related parameters, such as EI are calculated based on individual specimens with respect to the rebar used and specimen dimensions.

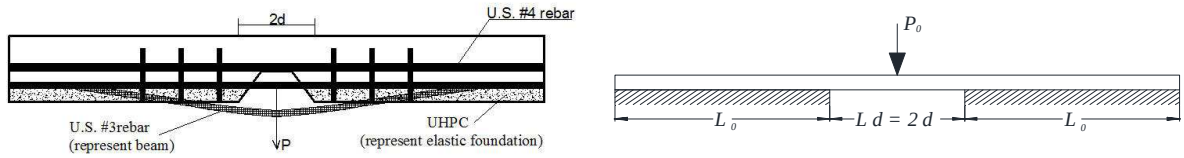

Figure 6: Test Setup and simplified model

Table 3: Curve fitting results of elastic foundation module

ID	Group 1	Group 2	Group 3	Group 4	Group 5
Peak Load (kN)	12.85	7.87	8.87	7.30	12.93
Module β	1.61	1.74	1.76	1.67	1.89

3.2 Beam on nonlinear foundation (BNF)

In order to predict the peak dowel action load, the beam on nonlinear foundation model (BNF) was introduced. Between the free span and elastic portion of the foundation, a perfect yielded region with reaction f_y was added, which means the foundation behaves nonlinearly as shown in Figure 7.

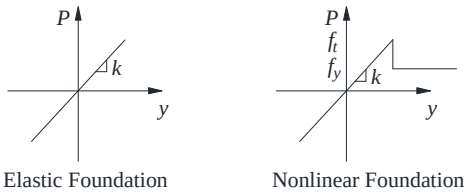

Figure 7: Load displacement model for linear and nonlinear foundation

The schematic drawing of the model is shown in Figure 8. The three segments of the nonlinear foundations were labeled as y_1, y_2, and y_3. The differential equations for the three regions are shown in Eq. (5).

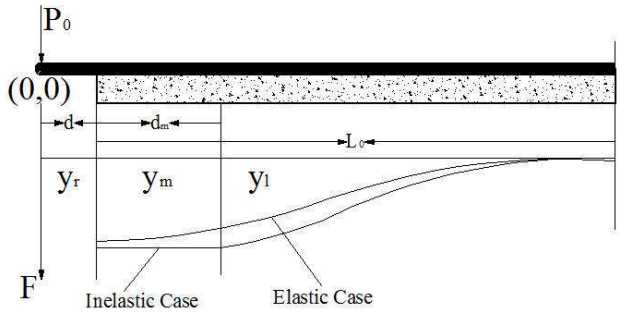

Figure 8: Schematic drawing of the BNF model

$$\begin{cases} EI\left(\frac{dy}{dx}\right)^4 = -ky & x\in[d+d_m,\infty) \\ EI\left(\frac{dy}{dx}\right)^4 = -f_y & x\in[d,d_m+d) \\ EI\left(\frac{dy}{dx}\right)^4 = 0 & x\in[0,d) \end{cases} \tag{5}$$

Solution of Eq. (5) is as follows,

$$\begin{cases} y_1 = \frac{1}{6}c_5x^3 + \frac{1}{2}c_6x^2 + c_7x + c_8 \\ y_2 = -\frac{1}{24}\frac{f_y x^4}{EI} + \frac{1}{6}c_9x^3 + \frac{1}{2}c_{10}x^2 + c_{11}x + c_{12} \\ y_3 = \frac{P_0\beta}{4k}\left[4e^{(-\beta x)}\cos(\beta x) - (2-\beta L_{d0})e^{(-\beta x)}\left(\cos(\beta x) - \sin(\beta x)\right)\right] \end{cases} \tag{6}$$

Parameter L_{d0} is the equivalent length of the free span for the right part. It can be calculated as $L_{d0} = L_d - f_y d_m^2 / P_0$ based on the equivalence of moment and shear force at the beginning of the portion 3. The six integration constants can be solved by similar boundary conditions as the elastic solutions. Two additional equations are introduced as follows:

$$f_t = \frac{P_0\beta(2+\beta L_{d0})}{4}\ ,\ f_y = \alpha f_t\left(1-\frac{\mathrm{d}_m}{L_0-d}\right) \tag{7}$$

The first equation ensures that the force at the beginning of portion 3 equals the critical cracking force f_t, and the second equation specifies the reduction function of the yielding force f_y with respect to the spreading width of the yielding portion. Parameter α is the factor taking care of the stress change at the onset of the cracking.

By specifying the numerical values of known parameters, the force versus d_m relation can be obtained, which shows the spreading of nonlinear foundation behavior away from the notch as the load is increased. This relation is a function of parameter α, which can be estimated based on the experiment results. The load versus yielding width d_m is shown in Figure 9. For all α values, the peak load happens around d_m = 100 *mm*, which is determined by the linear decay relation between f_y and d_m. Some modifications may need on this

assumption based on the verification of the recorded deflection data. The elastic foundation modulus β used in the calculation is the same for all groups and equals 1.7.

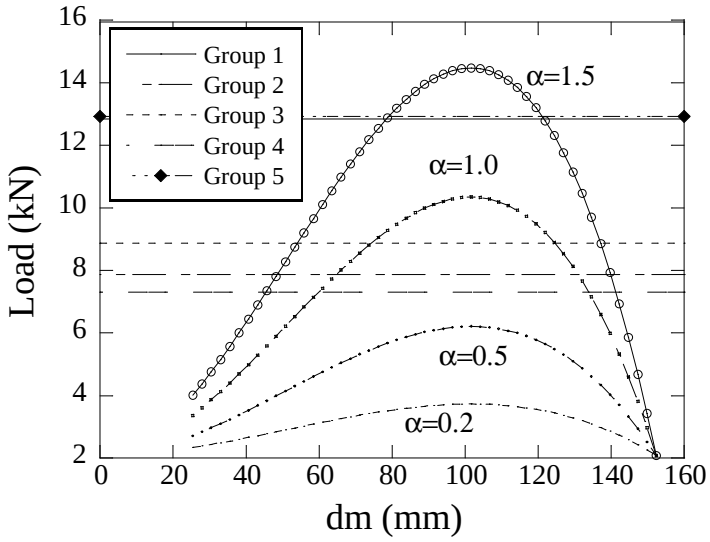

Figure 9: Load versus yielding range for various α values

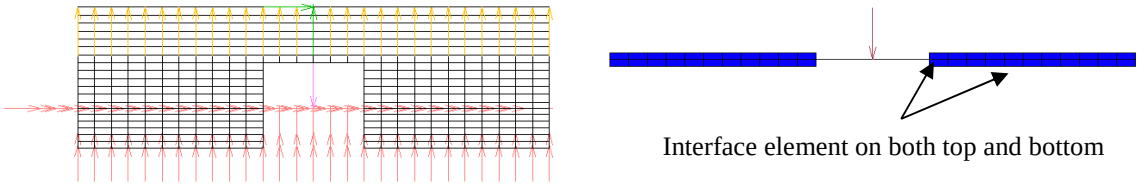

Meshing and Boundary Interface Connections

Figure 10: FEM model, Mesh and Interface

4. FINITE ELEMENT ANALYSIS

Three dimensional finite element analyses were performed using MSC.Mentat/Marc to investigate the dowel action response of the specimens. A low tension material was used in the model for UHPC with cracking stress equals *7.6 MPa* and the softening modulus set as *345 MPa*. The rebar was modeled by two-node closed section beam elements with nonlinear high strength steel material models as shown in Figure 10. Interface elements were used to connect the rebar element to the surrounding UHPC. In order to reflect the fact the interfacial shear strength is very small due to the use of the plastic tubes, the interface elements were set accordingly such that they are only able to sustain compressive stresses. At the same time, a small shear retention factor equal to 0.01 was used to prevent the shear force transfer after cracking. The FEM results for specimen 12 were compared to the experimental results as shown in Figure 11.

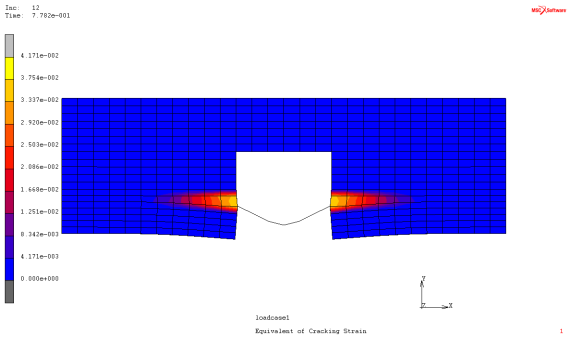

Crack distribution

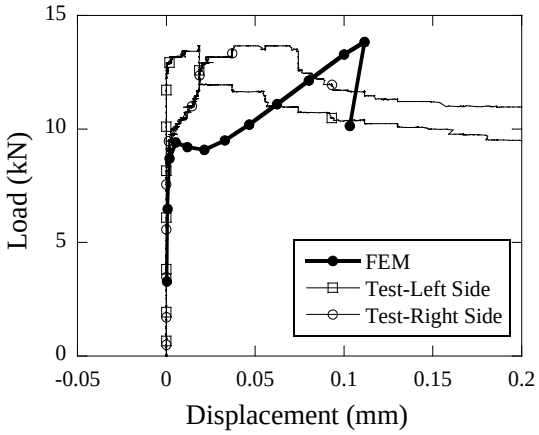

FEM versus test results at location 3.5*in*

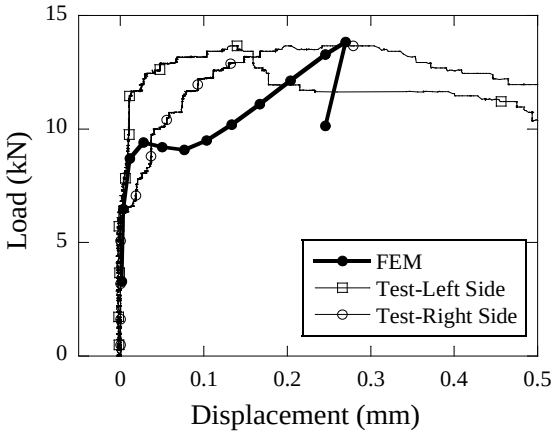

FEM versus test results at location 2.5 *in*

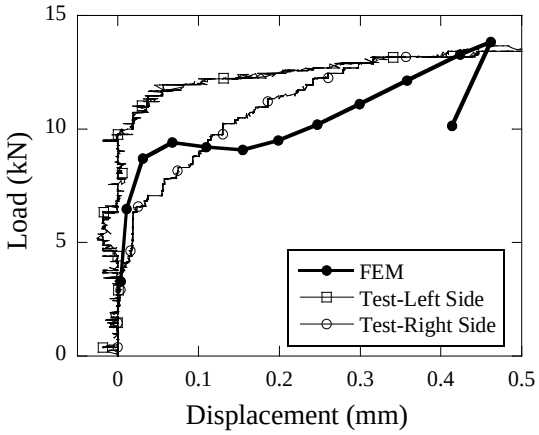

FEM versus test results at location 1.5 *in*

Figure 11: Results of FEM compared to experiment

5. CONCLUSION AND DISCUSSION

This paper investigated the dowel action between high strength rebar and surrounding UHPC. By using the separation plastic tubes, the test setup successfully obtained the peak dowel force without the influence of the interfacial bond. By use the beam on elastic foundation theory, the foundation modulus for case of rebar against UHPC cover was calibrated using the experimental displacement results. In order to capture the peak dowel force, the concept of nonlinear foundation was introduced. By assuming the decay relation between the foundation yielding length and the average post-crack tensile strength of UHPC, the peak load can be estimated based on the initial cracking strength. In order to fully understand the load transfer mechanism, a finite element model was built, and the load versus displacement curves at different measurement location along the length shown acceptable agreement with experiment results. Further investigation will aim at build the general model to predict the dowel action contribution on the shear strength based on the calibrated foundation modulus, yielding range, and decay conditions based on the parameters, such as rebar diameter, cover size, and bond length.

ACKNOWLEDGEMENTS

Authors are pleased to acknowledge the support of Lafarge North America who provided the materials for the UHPC (Ductal®). All experiments were conducted at the Structure's Testing Laboratory of the University of Central Florida.

REFERENCES

[1] Mirmiran, A., Saleem, M., Mackie, K. and Xia, J., 'Alternatives to steel grid decks'. 2009, Florida International University, University of Central Florida. p. 187.
[2] Mirmiran, A., Saleem, M., Mackie, K., Xia, J. and Xiao Y., 'Alternatives to steel grid decks--Phase II'. 2012, Florida International University, University of Central Florida. p. 93.
[3] Graybeal, B.A., 'Material Property Characterization of Ultra-High Performance Concrete'. 2006, Federal Highway Administration.
[4] Chanvillard, G. and Rigaud, S., 'Complete characterization of tensile properties of Ductal® UHPFRC according to the French recommendation', Proceedings of 4th Int. RILEM workshop on High Perormance Fiber Reinforced Cement Composites (HPFRCC4), Springer, The Netherlands.: Ann Arbor, Michigen,.
[5] Carpinteri, A., Chiaia, B., and Ferro, G., 'Size effect on nominal strength of concrete structures: Multifractality of material ligaments and dimensional transition from order to disorder'. *Materials and Structures* 1995. 28: p. 311-317.
[6] Ince, R. and Arici, E., 'Size effect in bearing strength of concrete cubes'. *Construction and Building Materials* 2004. 18(603-9).
[7] Ince, R., Yalcin, E., and Arslan, A., 'Size-dependent response of dowel action in R.C. members'. ScienceDirect, Engineering Structures 2006. 29: p. 955-961.
[8] Soroushian, P., 'Behavior of Bars in Dowel Action Against Concrete Cover'. *ACI Structural Journal* 1987. 84(2): p. 170-176.
[9] El-Ariss, B., 'Behavior of beams with dowel action'. *Engineering Structures*, 2007. 29(6): p. 899-903.
[10] Reineck, K.-H., 'Ultimate shear force of structural concrete members Without Transverse Reinforcement Derived From a Mechanical Model (SP-885) '. *ACI Structural Journal*, 1991. 88(5): p. 592-602.
[11] He, X.G. and Kwan, A.K.H., 'Modeling dowel action of reinforcement bars for finite element analysis of concrete structures'. *Computers & Structures*, 2001. 79(6): p. 595-604.
[12] Hetenyi, M., 'Beams on elastic foundation; theory with applications in the fields of civil and mechanical engineering' 1946: Ann Arbor, The University of Michigan press.